Chapter 7

OPTIMAL ADHESION CONTROL VIA COOPERATIVE HIERARCHY, GRADING, GEOMETRIES AND NON-LINEARITY OF ANCHORAGES AND ADHESIVE PADS

Lucas Brely[(1)], Daniele Liprandi[(1)], Federico Bosia[(1)], and Nicola M. Pugno[(2,3,4)*]

Department of Physics and "Nanostructured Interfaces and Surfaces" Centre, Università di Torino, Via P. Giuria 1, 10125, Torino (Italy).

(1) Laboratory of Bio-Inspired & Graphene Nanomechanics, Department of Civil, Environmental and Mechanical Engineering, Università di Trento, via Mesiano, 77, I-38123 Trento, Italy.

(2) Center for Materials and Microsystems, Fondazione Bruno Kessler, Via Sommarive 18, I-38123 Povo (Trento), Italy.

(3) School of Engineering and Materials Science, Queen Mary University of London, Mile End Road, London E1 4NS.

(*) Corresponding author: *nicola.pugno@unitn.it*

ABSTRACT

Optimization of dry **adhesion** in biological organisms is achieved using various strategies at different scale levels. In the past, studies have shown how contact splitting is used effectively by animals such as geckos and insects to increase the total peeling line of contacts and therefore adhesion force. Also, tapering of contacts or grading of their mechanical properties has been shown to be instrumental in the achievement of improved adhesion efficiency. On a more macroscopic scale, structures such as spider web anchorages exploit hierarchical structure or nonlinear constitutive material properties to improve resilience and to achieve tunability in adhesion/detachment characteristics. Here, we analyse some of these properties and propose some mechanisms for the optimization of adhesion that have thus far been neglected in modelling approaches, and could be potentially exploited for the design of bioinspired adhesives. We consider **hierarchical structure**, **contact tapering**, and **grading** of mechanical properties, and their interaction. It emerges that these mechanisms contribute on various size scales in achieving optimal adhesive properties through structural complexity and hierarchical organization.

Keywords: Adhesion, modelling, multiple peeling, bioinspired, gecko adhesion, spider web anchorages, contact splitting, contact tapering, Kendall theory, Griffith energy balance, thin film peeling, tunability, hierarchical structure, peeling line, peeling force, stress concentrations, Finite Element Analysis, grading, fibrillar structures, peeling angle.

1. INTRODUCTION

Natural structural materials have been widely used as a source of inspiration for advanced materials, due to their outstanding mechanical properties. This applies to the field of adhesives [1], where notable examples are **fibrillar structures** such as those found in gecko toe pads or in insects [2,3]. Another interesting example is that of spider web attachment discs, in which different types of spider silk threads and hierarchical branching are employed to tune adhesion for specific applications [4-6]. In all of these examples, material properties and structure concur in determining adhesive functionality. As for many natural materials, hierarchical structures are observed in many cases ("hierarchical branching"), and it is thought that these are essential in determining optimal adaptation to the surface, load redistribution without self-bunching and possibly tunability in adhesive properties [7]. This hierarchical branching allows so-called "**contact splitting**", whereby larger contacts are split into smaller ones (fibrils), with benefits deriving from fibril deformation, adaptability to rough surfaces, size effects due to surface-to-volume ratio, uniformity of stress distributions [8]. Contact splitting also contributes to increasing the so-called "peeling line", i.e. the sum of the contact tape widths, also increasing adhesion [7]. Additionally, it has been shown that in biological structures adhesion can be optimized by variable contact unit geometry [9] and spatial variation of mechanical properties, e.g. in the tarsal setae of the ladybird beetle, allowing it to achieve adaptation to rough surfaces while simultaneously ensuring sufficient stability [10]. These concepts are illustrated in Fig. 1, highlighting the multiscale nature of these mechanisms.

Artificial dry adhesives mimicking natural systems have recently been introduced [11]. For example, creating pillar (or mushroom)-shaped patterns at micro (and nano) scale has allowed to successfully activate adhesion based on Van Der Waals interactions. The first artificial "mushroom-tape" or "gecko tape" are based on a punch-like structure [12,13], which is designed to provide an adhesive force normal to the substrate. The optimization of these structures in terms of adhesive strength has been attempted using contact mechanics models [14]. As the size of the contact tip decreases, the models predict an unlimited increase in adhesive strength. Using nanoscale contact units, the adhesive strength tends to the theoretical strength of the Van der Waals interaction. On the other hand, most natural designs are based on a tape-like geometry, which can be described using **Kendall**'s "single peeling" theory [15] developed in the 1970ies, and recently extended to "multiple peeling" cases [16,17] and applied to complex geometries [18]. Tape-like structures were also introduced in artificial adhesives in order to optimize the shear mode adhesion of bioinspired tapes [19,20]. The study of how nature organizes these

basic constitutive units could lead to further optimization in the field of **bioinspired** adhesives. In this respect, introducing hierarchical structures instead of using regular patterns is the new challenge [21,22]. To design optimal solutions, adequate **modelling** of all mechanical mechanisms is required, and thus reliable analytical/numerical approaches need to be developed [23,24].

In this work, we analytically and numerically analyse various mechanisms that can contribute to improvement of adhesion at different scale levels, at present observed experimentally in the literature but not fully explained theoretically. These include the creation of favourable delamination stress distributions thanks to spatial stiffness variation of the fibrillar elements and increasing the **peeling line** and adhesion force through contact tapering, i.e. width or thickness variations along the pad length, and hierarchical organization of multiple peeling geometries. The study is performed through energy-based analytic calculations and stress distributions analysis. Finite Element Method (FEM) numerical simulations and their multiscale interaction in complex hierarchical multiple peeling geometries are finally discussed.

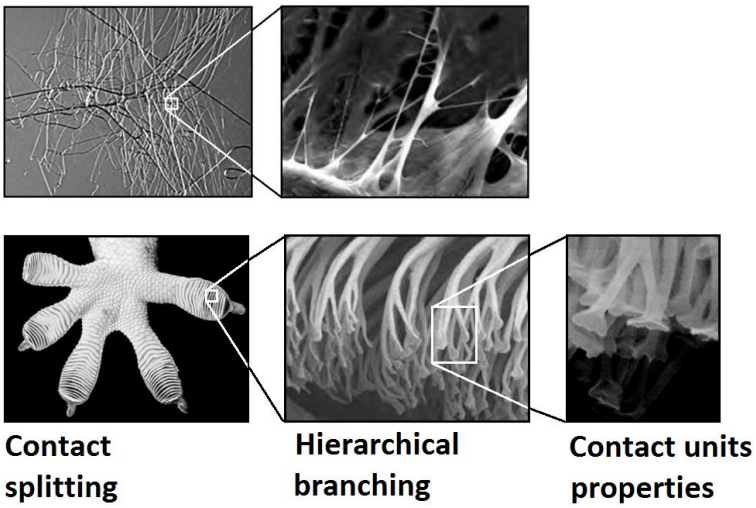

Figure 7-1: Multiscale mechanisms contributing to fibrillar adhesion: contact splitting, hierarchical branching, contact unit properties (i.e. tapering or grading of mechanical properties) (from [25,26]).

2. SINGLE AND MULTIPLE PEELING THEORIES APPLIED TO ATTACHMENT STRUCTURES

Adhesion problems in biological structures can usually be investigated by resorting to **thin film peeling** theories [15,16], due to the typical tape-like shape of the terminal contact units observed in systems such as gecko spatulae, insect setae, spider attachment discs, mussel adhesive plaques, etc. These typically involve multiple contact units, so that the detachment of adhesive biological structures must be treated as a multiple peeling problem. In this type of formulation, **Griffith energy balance** is used to determine whether the *k*-th tape of a structure delaminates or not:

$$-\partial \Pi / \partial l_k = 2\gamma_k w_k \tag{1}$$

where Π *is* the potential energy, given as the difference between the elastic energy E and the external work W, i.e. $\Pi = E - W$, γ is the surface energy between tape and surface, w_k the tape width and l_k its length. For a thin film (i.e., neglecting the bending stiffness), the variation of external work ΔW can be expressed as:

$$\Delta W = F \Delta \eta \tag{2}$$

Where F is the applied force and $\Delta\eta$ the increment in displacement. The elastic energy variation can be calculated as:

$$\Delta E = \frac{1}{2} \sum_{k=1}^{N} Y_k b_k \, w_k \left(l_k{}' \varepsilon_k'^2 - l_k \varepsilon_k{}^2 \right) \tag{3}$$

where Y_k is the *k*-th tape elastic modulus, b_k its thickness, w_k its width and ε_k\ its strain. l_k' and ε_k' correspond to the length and the strain in the delaminated configuration (see Fig. 2a) . For a single tape (Fig. 2b), the force necessary to peel the film from a substrate can be analytically obtained[15]:

$$T(1 - cos\,\theta) + \frac{T^2}{2bwY} - 2\gamma w = 0 \tag{4}$$

where T is the tape tension, θ is the tape angle with respect to the substrate, and the subscript k has been dropped for simplicity. This leads to:

$$T = wbY \left(\cos\theta - 1 + \sqrt{(1 - \cos\theta)^2 + \frac{4\gamma}{bY}} \right) \tag{5}$$

which highlights the proportionality of the peeling force with the tape width *w*. This geometrical parameter is linked to the width of the peeling line, i.e. the line along which delamination occurs. As discussed in [7], a well-known strategy adopted by biological attachments systems consists in increasing the length of peeling line by simply splitting the contacts. This result is illustrated by the log relationship between the body mass and the sum of the peeling lines in animal fibrillar attachment structures [7].

In the case of **multiple peeling** problems, we first consider symmetrical double peeling, as shown in Fig. 2c, since asymmetrical cases can be treated as combined single peeling problems [18]. The applied force is the decomposition of the tape tensions, which leads to:

$$F = 2\,T\,sin\,\theta \tag{6}$$

so that at delamination ($F = F^*$, $\theta = \theta^*$):

$$F^* = 2wbY\,sin\,\theta^*\left[cos\,\theta^* - 1 + \sqrt{(1 - cos\,\theta^*)^2 + \frac{4\gamma}{bY}}\right] \tag{7}$$

In this case, the angle between the tapes and the substrate changes with the tape elastic deformation. Solving Eq. (7), one finds that an optimal peeling angle exists at which the peeling force is maximal. For angles below and above this value, the peeling force decreases. However, in Eq. (7) the peeling force is expressed as a function of the delamination (or "peeling") angle θ^*, so that **peeling angle** values below the optimal value correspond to negative "undeformed" initial angles θ_0, which is physically meaningless. The tape tension can be expressed from the tape strain as $l(1+\varepsilon)\cos\theta = l\cos\theta_0$, so that:

$$T = bwY\varepsilon = bwY\left(\frac{\cos\theta_0}{\cos\theta} - 1\right) \tag{8}$$

while the external load applied to the system is given by Eq. (6). Considering as an example a tape with properties Y_k = 1000 MPa, b_k = 1 µm, w_k = 2 µm, γ_k = 0.01 MPa.µm or γ_k = 0.001 MPa.µm, calculations shown in Fig. 3a demonstrate that the peeling force F reaches a maximum when its intersects the peeling force F^* calculated as a function of angle variation when the initial tape angle is $\theta_0 = 0$ [18]. Indeed, the peeling force cannot be greater than the external load applied to the system for a given tape deformation. An initial undeformed angle of θ_0=0 degrees is therefore the optimal peeling angle for maximized adhesion force.

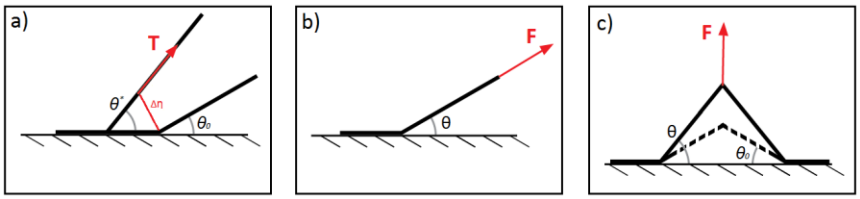

Figure 7-2: a) Tape angle before deformation ($\theta = \theta_0$) and at delamination ($\theta = \theta^*$) due to a tape tension T. b) Single peeling configuration with an applied force F (in which case $\theta_0 = \theta^*$). c) Symmetrical double peeling configuration with a vertically applied Force F: undeformed (θ_0) and deformed ($\theta<\theta^*$) tape angle.

The optimal **peeling angle** is a function of the global deformability of the system, i.e. the deformation that the system can sustain before delamination occurs. This property can be quantified using the non-dimensional parameter $\lambda = \frac{4\gamma}{bY}$ representing the ratio between adhesion energy and elasticity [16]. From Eq. (7) and Eq. (8), it is possible to determine the optimal peeling angle $\theta^{opt} = \theta^*|_{\theta_0=0}$ at which the structure delaminates for an optimal geometry ($\theta_0 = 0$):

$$2\cos^3\theta^{opt} - (3+\lambda)\cos^2\theta^{opt} + 1 = 0 \tag{9}$$

The corresponding θ^{opt}vs. λ curve is shown in Fig 3b, showing a monotonically increasing nonlinear behaviour. More in general, we have:

$$\cos\theta_0 = \cos^2\theta^* + \cos\theta^*\sqrt{(1-\cos\theta^*)^2 + \lambda} \tag{10}$$

Using this relation, it is possible to plot the **peeling force** as a function of the undeformed angle θ_0 (Fig. 3c). These results highlight the fact that in multiple peeling cases, delamination is dependent from the deformability of the system, and therefore from the type of structure and the mechanical properties of the attachment.

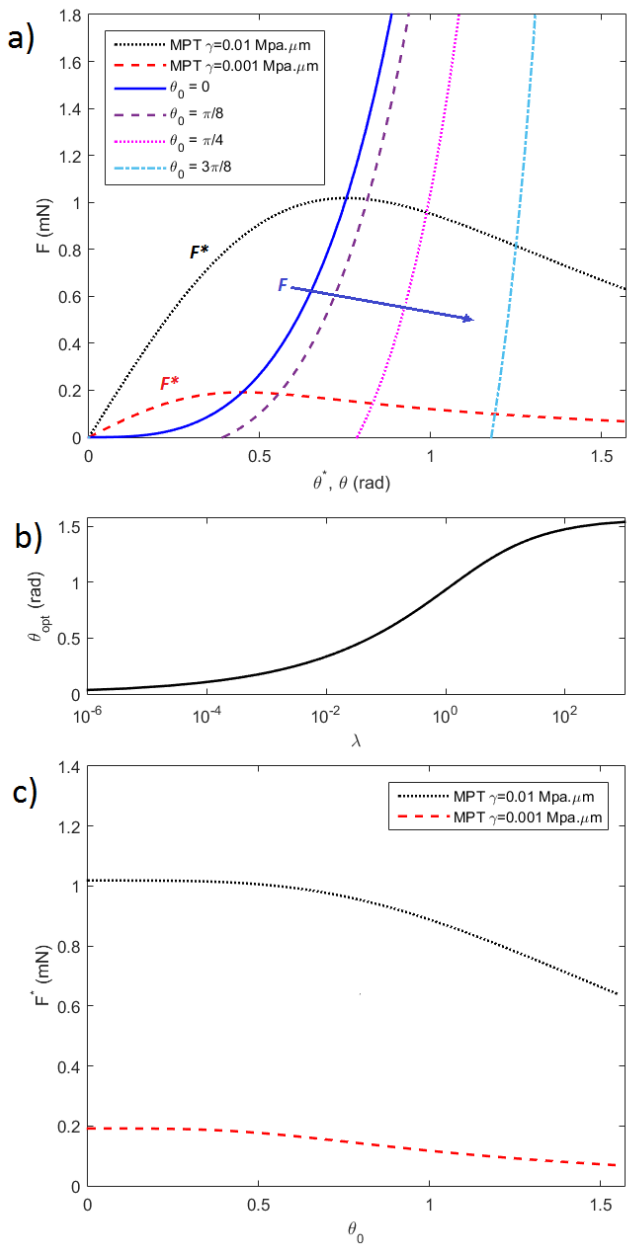

Figure 7-3: a) Peeling force F^* as a function of deformed tape angle θ, calculated with Multiple Peeling Theory (MPT, Eq.7), compared to the external load F applied to the system as a function of θ (Eq.8) for various initial angles. The $\theta_0 = 0$ curve is the one that intersects the MPT curve for maximal peeling force values. b) Optimal peeling angle θ_{opt} for symmetric double peeling as a function of the ratio between adhesion energy and elasticity of the system. c) Peeling force F^* as a function of the initial angle θ_0.

The adhesion force of attachment structures can be deduced from planar multiple peeling models such as those discussed above. One example are so-called "dendritic" geometries in **spider web anchorages**, which can be described as radial branching structures where the pyriform silk fibres converge to a single point at a distance from the substrate. This results in a cone-like morphology (Fig. 1) which is involved in spider prey capture. It has been shown that in order to fulfil its function, the dendritic anchorage must exhibit a reduced pull off force [4,27]. Due to its conical symmetry, the relationship between force and extension can be directly obtained from the symmetric double peeling configuration described above, modified by multiplying results by the appropriate number of tapes. Fig. 4a shows simulations results for dendritic attachments when varying the initial contact angle θ_0. For $\theta_0 = \pi/4$, the system is firstly deformed without delamination, with a linear force-displacement relationship (Hooke's law). Then, the tapes begin to delaminate and the peeling angle starts to vary, which results in an increase of the peeling force. This explains the elasto-plastic-like behaviour obtained in experimental [5] and in numerical results. The peeling force saturates when the peeling angle is optimal. In the case of a limited available delamination length, however, full delamination could be achieved before the optimal peeling angle, and thus before the load plateau, is reached. This would allow to **tune** the adhesive strength of the structure. For a small peeling angle ($\theta_0 = \pi/16$), the initial elastic deformation displays hyperelastic behaviour due to the geometrical non linearity of the system, but then saturates to the maximum peeling force as soon as delamination begins. These two cases illustrate how by varying the peeling angle and attached tape lengths, it is possible to control the properties of the anchorage, inducing linear/nonlinear deformation and varying detachment loads. The possibility of tuning load response by selecting suitable multiple peeling structures has been observed experimentally, e.g. in spider web anchorages [5]. In more complex loading scenarios, such as when applied loads are not normal to the surface, asymmetric deformation states are induced (as shown in Fig. 4b), and FEM approaches are necessary to evaluate the performance of these structures.

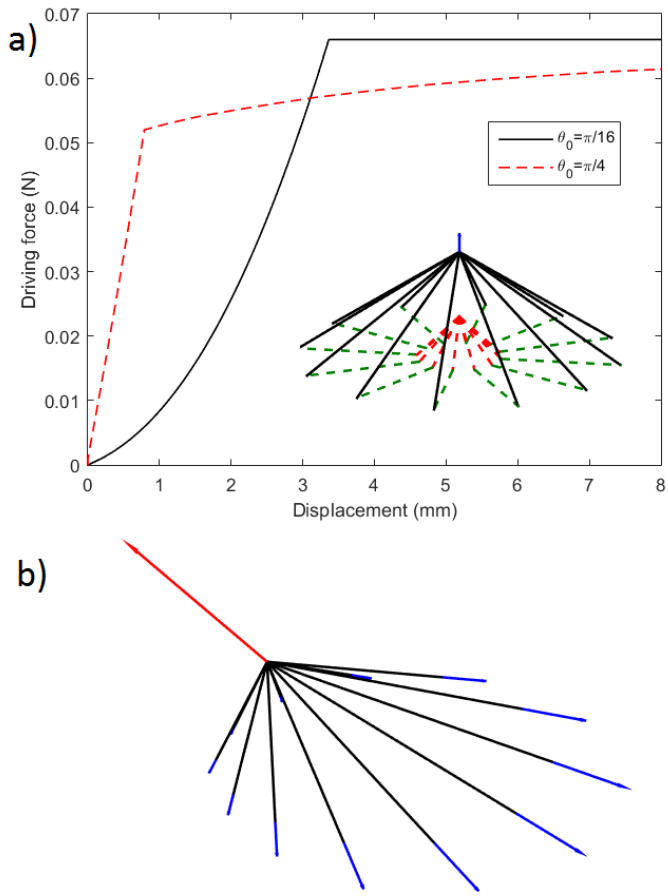

Figure 7-4: a) Force-extension curves for a dendritic anchorage, varying peeling θ_0 of the anchorage. b) Model of dendritic anchorage in an asymmetric loading scenario.

3. HIERARCHICAL BRANCHING IN ADHESIVE STRUCTURES

Adhesive fibrillar structures found in Nature display much more complex geometries than the double peeling problem discussed above. One example is the branched structure found in spider attachment discs, where a high number of contacts with the substrate are obtained thanks to hierarchical structure and branching at several levels [5,28], as illustrated in Fig. 1. To evaluate 2-D branched hierarchical multiple peeling configurations, **FEM** simulations have been carried out using the Structural Mechanics module of COMSOL

Multiphysics 4.3. The interface between the tape and substrate is modelled adopting a Cohesive Zone Model (CZM) [29], based on a stress-softening constitutive law before delamination [24]. Simulation parameters are $b = 10^{-2}$ m, $t = 10^{-3}$ m, $Y = 3$ MPa, $\nu = 0.45$ (where ν is the Poisson's ratio). The hierarchical configurations are compared to the symmetrical double peeling case. A second-level hierarchical geometry is considered ("2"), where the two tapes branch out in a self-similar manner into two further tapes at equal distances from the centre. The third-level hierarchical geometry ("3") replicates this to a further level. These structures are shown in Fig. 5a, with the corresponding calculated load-displacement curves in Fig. 5b. The three configurations are compared for the same peeling line, length, and thickness, and all three start from a fully adhered tape. It is apparent that increasing **hierarchical branching** increases contact splitting and the number of delamination points in the tape, thus distributing and reducing the stresses at the interface. This helps in avoiding **stress concentrations** and an early onset of tape delamination. On the other hand, tape deformation and internal stresses are generally greater. The variation in normalized adhesive properties of the three structures is reported in Fig 5c. There is an increase in adhesive stresses with hierarchy, i.e. the geometry with the highest hierarchical level achieves the best adhesive strength. Also, dissipated energy, which can be obtained as the area underlying the load-displacement curves, also increases for 2 and 3, showing how hierarchy favours an increase in both the strength and toughness of the adhesive interface.

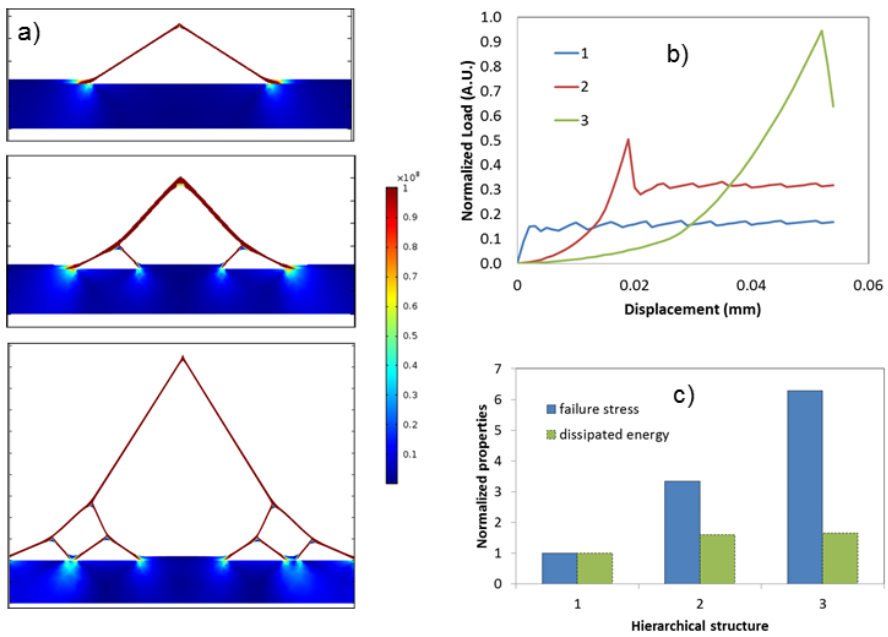

Figure 7-5: Hierarchical peeling configurations: a) FEM simulation results, pictured for different imposed displacement δ values. 1: first level (non-hierarchical) configuration; 2: second-level hierarchy; 3: third-level hierarchy. Colour scale represents Von Mises stresses during delamination (scale bar shown on the left). b) Corresponding Load vs. displacement curves: the peaks in the curves correspond to full delamination of single tapes; c) Comparison between the normalized delamination stress and dissipated energy at delamination for the 3 configurations.

4. GEOMETRY AND MECHANICAL PROPERTIES OF CONTACT UNITS

At a lower scale level, the peeling force of a single tape depends on the mechanical properties and the geometry of the contact unit itself. It is well known that the **gecko** spatulae or insect setae are not simple uniform tapes, but display gradients in the mechanical properties along both the width and the thickness of the attached length [10]. It has been shown that due to the concentration variation of a softener, the resilin protein, the elastic modulus in the adhesive tarsal setae of the ladybird beetle varies approximately from 1 MPa to 6 GPa, with two gradients, one along the length of the setae, the other along its thickness, in the dorsal (in contact with the substrate) and ventral part of the setae [10]. This result cannot be justified simply using Kendall's theory, which predicts that the peeling force increases with the elastic modulus. The softening has the function to increase adaptability to the surface, which leads

to a greater contact area, and an increase in adhesive energy. However, stress distributions on the contact area should also be considered to determine the possibility of early-stage onset of delamination in correspondence with **stress concentrations**. These effects can be captured using the stress distributions in the tape / interface system theoretically derived in [30]. The shear and normal stress (τ and σ) distributions at the interface are:

$$\tau(x) = T\cos(\theta)\frac{\alpha}{w}e^{\alpha x} \tag{11}$$

and

$$\sigma(x) = T\sin(\theta)\frac{2\beta}{w(1-K)}e^{\beta x}(\cos(\beta x) + K\sin(\beta x)) \tag{12}$$

where x is the distance from the peeling line, α β and K are parameters that depend on geometry and mechanical properties:

$$\alpha = \sqrt{\frac{G_I}{Y_t ab}}; \quad \beta = \sqrt[4]{\frac{3Y_I}{Y_t ab^3}};$$
$$K = 1 - \frac{\sin(\theta)}{\sqrt{2Y_t I_t(1-\cos(\theta))/T - \beta b/2\cos(\theta) + \sin(\theta)}} \tag{13}$$

where G_I and Y_I are the interface shear and elastic modulus, G_t and Y_t the tape interface shear and elastic modulus, I_t its momentum of inertia, and a the interface thickness. Considering an interface of setae with fixed mechanical parameters, the shear stress distribution can be derived approximately using Eq. (11). Gradually reducing the interface stiffness allows to distribute the stress over a larger area and therefore to increase the adhesive strength of the attachment. This is shown in Fig.6a, where results are calculated using the same mechanical properties as in the first Section and the geometry shown in the inset. For the sake of simplicity, we only plot the shear stress distribution considering $\theta = 0$ and applying a force $T = 0.1$ μN. We consider both the tape and interface to be isotropic, so that $G=Y/2(1+\nu)$, with $\nu = 0.3$. Shear stress along the length of the adhesive area for various stiffness values of the soft interface Y_I compared to that of the elastic layer Y_t are plotted in Fig. 6a. Results show how layer softening can have a considerable beneficial effect in reducing stress concentrations towards the tip of the pad, redistributing them more uniformly along the whole length of the interface area. For the same applied external force, in the considered case a 10-fold reduction can be obtained in the normal stresses, with an approximately equivalent increase in the adhesive strength of the layer. Another simple strategy to tune the adhesive strength is to generate **tapered geometries**. Indeed, most of the observed setal

elements in insects and geckos display a width variation over the length of the setae [9]. As predicted by **Kendall's** model, these structures would increase the adhesive strength as the delamination proceeds, thanks to the increasing **peeling line** length (Fig. 6b) [7]. These broadened contact units are characteristic features observed not only in gecko adhesion systems [31], but also in those of spiders [32].

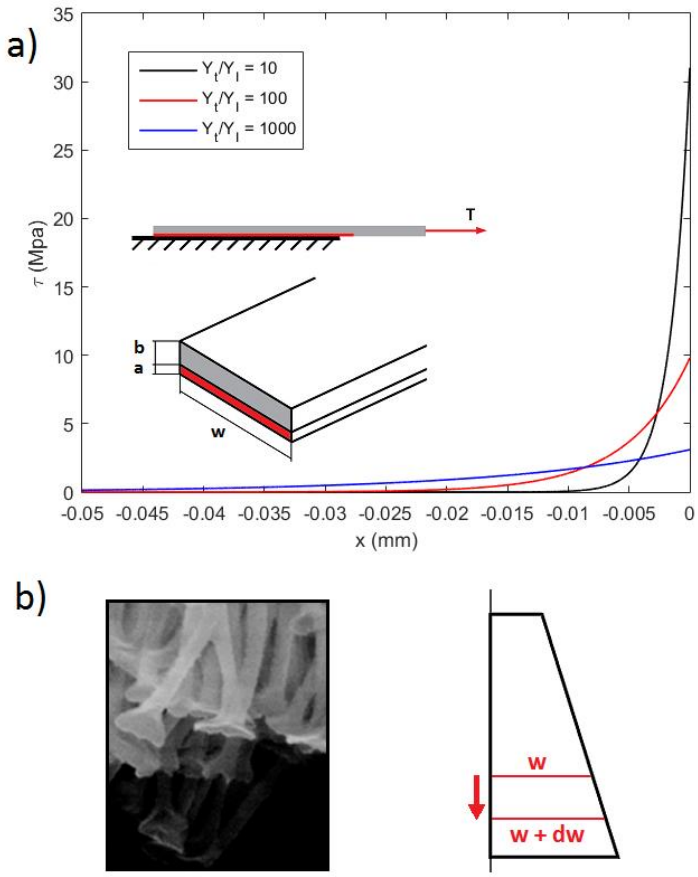

Figure 7-6: a) Geometry of the considered a thin elastic layer with a "ventral" soft interface and an applied horizontal force *T*. Shear stress distributions are plotted along the length of the attached region for varying ratios between contact layer stiffness Y_I and tape stiffness Y_t. Softer contact layers are shown to reduce stress concentrations with respect to stiffer layers. b) tapered geometry of terminal contact element width to increase peeling line ($w \rightarrow w+dw$) during delamination (image from [25])

5. CONCLUSIONS

In summary, we have reviewed how structural, geometric and mechanical features contribute on different scale levels to optimizing adhesion in biological adhesives. Many of these effects have been observed experimentally in the literature and discussed qualitatively, but we have demonstrated how they can also be derived analytically and numerically, based on Multiple Peeling Theory, its numerical implementation and FEM-based simulations. These features can readily be applied to artificial adhesives, e.g. "mushroom"-like structured surfaces [12,33,34], using the developed numerical tools for structural, geometrical and mechanical optimization. The observed effects can contribute on different scale levels, with cumulative optimization of adhesive properties. For example, in the considered cases of branched hierarchical structures, tapering or contact softening in the terminal elements could provide additional multiplier effects in the enhancement of the adhesion force. Future studies can exploit the proposed approach to further elucidate in a multiscale scheme the observed strategies found in Nature for adhesion optimization and their interaction, and propose new structural designs for artificial adhesives.

ACKNOWLEDGEMENTS

N.M.P. is supported by the European Research Council (ERC StG Ideas 2011 BIHSNAM n. 279985, ERC PoC 2015 SILKENE n. 693670), and by the European Commission under the Graphene Flagship (WP14 Polymer Composites, no. 696656). LB and FB acknowledge support from BIHSNAM. Computational resources were provided by HPC@POLITO, a project of Academic Computing within the Department of Control and Computer Engineering at the Politecnico di Torino (http://www.hpc.polito.it).

REFERENCES

[1] A. M. Smith and J. A. Callow, *Biological adhesives* (Springer, Berlin ; New York, 2006).
[2] K. Autumn and A. M. Peattie, Integr Comp Biol **42**, 1081 (2002).
[3] H. Yao and H. Gao, J Mech Phys Solids **54**, 1120 (2006).
[4] V. Sahni, T. A. Blackledge, and A. Dhinojwala, J Adhesion **87**, 595 (2011).
[5] V. Sahni, J. Harris, T. A. Blackledge, and A. Dhinojwala, Nat Commun **3**, 1106 (2012).
[6] I. Grawe, J. O. Wolff, and S. N. Gorb, J R Soc Interface **11** (2014).

[7] M. Varenberg, N. M. Pugno, and S. N. Gorb, Soft Matter **6**, 3269 (2010).
[8] M. Kamperman, E. Kroner, A. Del Campo, and McMeekin, Adv Eng Mater **12**, 335 (2010).
[9] A. Pantano, N. M. Pugno, and S. Gorb, Int J Fracture **171**, 169 (2011).
[10] H. Peisker, J. Michels, and S. N. Gorb, Nat Commun **4** (2013).
[11] A. K. Geim, S. V. Dubonos, I. V. Grigorieva, K. S. Novoselov, A. A. Zhukov, and S. Y. Shapoval, Nat Mater **2**, 461 (2003).
[12] G. Carbone, E. Pierro, and S. N. Gorb, Soft Matter **7**, 5545 (2011).
[13] M. Piccardo, A. Chateauminois, C. Fretigny, N. M. Pugno, and M. Sitti, J R Soc Interface **10** (2013).
[14] K. L. Johnson, K. Kendall, and A. D. Roberts, P Roy Soc A-Math Phy **324** 1558 (1971).
[15] K. Kendall, J Phys D Appl Phys **8**, 1449 (1975).
[16] N. M. Pugno, Int J Fract **171** 185 (2011).
[17] L. Afferrante, G. Carbone, G. Demelio, and N. M. Pugno, Tribol Lett **52**, 439 (2013).
[18] L. Brely, F. Bosia, and N. M. Pugno, Interface Focus **5**, 20140051 (2015).
[19] L. Qu, L. Dai, M. Stone, Z. Xia, and Z. L. Wang, Science **322**, 238 (2008).
[20] M. P. Murphy, B. Aksak, and M. Sitti, Small **5**, 170 (2009).
[21] H. E. Jeong, J. K. Lee, H. N. Kim, S. H. Moon, and K. Y. Suh, Proc Natl Acad Sci **106**, 5639 (2009).
[22] M. P. Murphy, S. Kim, and M. Sitti, ACS Appl. Mater. Interfaces **1**, 849 (2009).
[23] R. A. Sauer and M. Holl, Comput Method Biomec **16** 577 (2013).
[24] F. Bosia, S. Colella, V. Mattoli, B. Mazzolai, and N. M. Pugno, RSC Advances **4**, 25447 (2014).
[25] C. Guo, J. Sun, Y. Ge, W. Wang, D. Wang, and Z. Dai, Sci China Life Sci **55**, 181 (2012).
[26] Y. Hsia, E. Gnesa, F. Jeffery, S. Tang , and C. Vierra, in *Metal, Ceramic and Polymeric Composites for Various Uses* (J. Cuppoletti, 2011), pp. 303.
[27] S. W. Cranford, A. Tarakanova, N. M. Pugno, and M. Buehler, Nature **482**, 72 (2012).
[28] J. O. Wolff, I. Grawe, M. Wirth, A. Karstedt, and S. Gorb, Soft Matter **11**, 2394 (2015).
[29] M. Elices, G. V. Guinea, J. Gomez, and Planas, Eng Fract Mech **69**, 137 (2002).
[30] D. H. Kaelble, T Soc Rheol **4** 45 (1960).
[31] N. W. Rizzo, et al., N. W. Rizzo, K. H. Gardner, D. J. Walls, N. M. Keiper-Hrynko, T. S. Ganzke, and D. L. Hallahan, J R Soc Interface **3**, 441 (2006).
[32] A. B. Kesel, A. Martin, and T. Seidl, Smart Mater Struct **13**, 512 (2004).
[33] A. V. Spuskanyuk, McMeeking, R.M., Deshpande, V.S. & Arzt, E., Acta Biomater **4**, 1669 (2008).

[34] L. Heepe, A. E. Kovalev, A. E. Filippov, and S. Gorb, Phys Rev Lett **111**, 104301 (2013).